

COMPUTATION OF EXTERIOR MODULI OF QUADRILATERALS

HARRI HAKULA, ANTTI RASILA, AND MATTI VUORINEN

ABSTRACT. We study the problem of computing the exterior modulus of a bounded quadrilateral. We reduce this problem to the numerical solution of the Dirichlet-Neumann problem for the Laplace equation. An algorithm and its implementation with hp -FEM is documented. Several experimental results, with error estimates, are reported.

1. INTRODUCTION

A bounded Jordan curve in the complex plane divides the extended complex plane $\mathbb{C}_\infty = \mathbb{C} \cup \{\infty\}$ into two domains D_1 and D_2 , whose common boundary it is. One of these domains, say D_1 , is bounded and the other one is unbounded. The domain D_1 together with four distinct points z_1, z_2, z_3, z_4 in ∂D_1 , which occur in this order when traversing the boundary in the positive direction, is called a quadrilateral and denoted by $(D_1; z_1, z_2, z_3, z_4)$.

By Riemann's mapping theorem, the domain D_1 can be mapped conformally onto a rectangle $f: D_1 \rightarrow (0, 1) \times (0, h)$ such that the four distinguished points are mapped onto the vertices of the rectangle $f(z_1) = 0$, $f(z_2) = 1$, $f(z_3) = 1 + ih$, $f(z_4) = ih$. The unique number h is called the (conformal) modulus of the quadrilateral $(D_1; z_1, z_2, z_3, z_4)$. Apart from its theoretical significance in geometric function theory, the conformal modulus is closely related to certain physical quantities which also occur in engineering applications. In particular, the conformal modulus plays an important role in determining resistance values of integrated circuit networks (see e.g. [22, 23]). Similarly, one can map D_2 , the complementary domain, conformally $g: D_2 \rightarrow (0, 1) \times (0, k)$ such that the four boundary points are mapped onto the vertices of the rectangle $g(z_1) = 0$, $g(z_2) = 1$, $g(z_3) = 1 + ik$, $g(z_4) = ik$, reversing the orientation. Again the number k is unique and it is called the exterior modulus of $(D_1; z_1, z_2, z_3, z_4)$. In practice, the computation of both the modulus and the exterior modulus is carried out by using numerical methods such as numerical conformal mapping. Mapping problems involving unbounded domains likewise are related to some well known engineering applications such as determining two dimensional potential flow around a cylinder, or an airfoil.

In the case of domains with polygonal boundary, numerical methods based on the Schwarz-Christoffel formula have been extensively studied, see [10]. The literature and software dealing with numerical conformal mapping problems is very wide, see

File: hrv2.tex, printed: 2012-1-17, 4.21

1991 *Mathematics Subject Classification.* 65E05, 31A15, 30C85.

Key words and phrases. conformal capacity, conformal modulus, quadrilateral modulus, hp -FEM, numerical conformal mapping.

e.g. [10] and [22]. In our earlier paper [14] we applied an alternative approach which reduces the problem to the Dirichlet-Neumann problem for the Laplace equation. Thus any software capable of solving this problem may be used. We use the hp -FEM method for computing the modulus of a bounded quadrilateral and here we will apply the same method for the exterior modulus and another method, AFEM, for the sake of comparison, as in [14]. Our approach also applies to the case of domains bounded by circular arc boundaries as we will see below. It should be noted that while our method does not require finding the canonical conformal mapping, it is possible to construct the mapping from the potential function. An algorithm, with several numerical examples, is presented in [13].

In particular, an important example of a quadrilateral $(D_1; z_1, z_2, z_3, z_4)$ is the case when D_1 is a polygon with z_1, z_2, z_3, z_4 as the vertices and its modulus was computed in [15] and this formula was also applied in [14]. Here we reduce its exterior modulus to the (interior) modulus by carrying out a suitable inversion which keeps three vertices invariant and maps the exterior to the interior of a bounded plane region whose boundary consists of four circular arcs.

We apply here three methods to study our basic problem:

- (1) The hp -FEM method introduced in [14] and its implementation by H. Hakula.
- (2) The AFEM method of K. Samuelsson, see e.g. [7] and [14].
- (3) The Schwarz-Christoffel Toolbox of T. Driscoll and N. Trefethen [9, 10, 26, 27].

The methods (1) and (2) are based on a reduction of the exterior modulus problem to the solution of the Dirichlet-Neumann problem for the Laplace equation in the same way as in [1] and [14] whereas (3) makes use of numerical conformal mapping methods. Note that [1] also provides a connection between the extremal length of a family of curves and its reciprocal, the modulus of a curve family, both of which are widely used in the geometric function theory.

We describe the high-order p -, and hp -finite element methods and report the results of numerical computation of the exterior moduli of a number of quadrilaterals. In the p -method, the unknowns are coefficients of some polynomials that are associated with topological entities of elements, nodes, sides, and the interior. Thus, in addition to increasing accuracy through refining the mesh, we have an additional refinement parameter, the polynomial degree p . For an overview of the hp -method, see e.g. Babuška and Suri [6]. A more detailed exposition of the methods is given in [24, 25].

Our study is structured according to a few particular cases. We start out with the case when the quadrilateral is the complement of a rectangle and the vertices are the distinguished points of the quadrilateral. In this case we have the formula of P. Duren and J. Pfaltzgraff [11] to which we compare the accuracy of each of the above methods (1)-(3). Then we consider the problem of minimizing the exterior modulus of a trapezoid with a fixed height h and fixed lengths for the pair of parallel opposite sides and present a conjecture supported by our experiments. We also remark that the case of symmetric hexagons can be dealt with the Schwarz-Christoffel transformation and relate its exterior modulus to a symmetry property of the modulus of a curve family. Finally, we study the general case and present comparisons of (1)-(3) for this case as well. SC Toolbox does not have a built in function for computing the

exterior modulus. However, we use the function `exterm`, and an auxiliary Möbius transformation, to map the exterior of a quadrilateral $(D; a, b, c, d)$ conformally onto the upper half-plane so that the boundary points a, b, c and d are mapped to the points $\infty, -1, 0$ and $t > 0$, respectively. Then the exterior modulus of the quadrilateral is $\tau(t)/2$, where τ is the Teichmüller modulus function (see [2]). We use the MATLAB code from [2] to compute values of $\tau(t)$, $t > 0$.

At the end of the paper we present conclusions concerning the performance of these methods and our discoveries.

2. PRELIMINARIES

In this section we give reference results which can be used in obtaining error estimates. We also present some geometric identities which are required in our computations.

2.1. The hypergeometric function and complete elliptic integrals. Given complex numbers a, b , and c with $c \neq 0, -1, -2, \dots$, the *Gaussian hypergeometric function* is the analytic continuation to the slit plane $\mathbb{C} \setminus [1, \infty)$ of the series

$$(2.2) \quad F(a, b; c; z) = {}_2F_1(a, b; c; z) = \sum_{n=0}^{\infty} \frac{(a, n)(b, n)}{(c, n)} \frac{z^n}{n!}, \quad |z| < 1.$$

Here $(a, 0) = 1$ for $a \neq 0$, and (a, n) is the *shifted factorial function* or the *Appell symbol*

$$(a, n) = a(a+1)(a+2) \cdots (a+n-1)$$

for $n \in \mathbb{N} \setminus \{0\}$, where $\mathbb{N} = \{0, 1, 2, \dots\}$ and the *elliptic integrals* $\mathcal{K}(r), \mathcal{K}'(r)$ of the first kind are

$$\mathcal{K}(r) = \frac{\pi}{2} F(1/2, 1/2; 1; r^2), \quad \mathcal{K}'(r) = \mathcal{K}(r'), \text{ and } r' = \sqrt{1-r^2},$$

and the *elliptic integrals* $\mathcal{E}(r), \mathcal{E}'(r)$ of the second kind are

$$\mathcal{E}(r) = \frac{\pi}{2} F(1/2, -1/2; 1; r^2), \quad \mathcal{E}'(r) = \mathcal{E}(r'), \text{ and } r' = \sqrt{1-r^2}.$$

Some basic properties of these functions can be found in [2, 21].

2.3. The modulus of a curve family. For a curve family Γ in the plane, we use the notation $M(\Gamma)$ for its modulus [20]. For instance, if Γ is the family of all curves joining the opposite b -sides within the rectangle $[0, a] \times [0, b]$, $a, b > 0$, then $M(\Gamma) = b/a$. If we consider the rectangle as a quadrilateral Q with distinguished points $a+ib, ib, 0, a$ we also have $M(Q; a+ib, ib, 0, a) = b/a$, see [1, 20]. Given three sets D, E, F we use the notation $\Delta(E, F; D)$ for the family of all curves joining E with F in D .

2.4. The Duren-Pfaltzgraff formula [11, Theorem 5]. For $k \in (0, 1)$ write

$$\psi(k) = \frac{2(\mathcal{E}(k) - (1-k)\mathcal{K}(k))}{\mathcal{E}'(k) - k\mathcal{K}'(k)}.$$

Then $\psi: (0, 1) \rightarrow (0, \infty)$ defines an increasing homeomorphism with limiting values $0, \infty$ at $0, 1$, respectively. In particular, $\psi^{-1}: (0, \infty) \rightarrow (0, 1)$ is well-defined. Let R

be a rectangle with sides of lengths a and b , respectively, and let Γ be the family of curves lying outside R and joining the opposite sides of length b . Then

$$(2.5) \quad \mathbf{M}(\Gamma) = \frac{\mathcal{K}'(k)}{2\mathcal{K}(k)}, \quad \text{where } k = \psi^{-1}(a/b).$$

See also W.G. Bickley [8, (1.17) p. 86].

2.6. Circle through three points. First we find the equation of the circle $(x - x_0)^2 + (y - y_0)^2 = r^2$ through the points $z_j = x_j + iy_j$, $j = 1, 2, 3$. It is well known that

$$x_0 = -\frac{d}{2c}, \quad y_0 = -\frac{e}{2c}, \quad \text{and } r = \sqrt{\frac{d^2 + e^2}{4c^2} - \frac{f}{c}},$$

where

$$c = \begin{vmatrix} x_1 & y_1 & 1 \\ x_2 & y_2 & 1 \\ x_3 & y_3 & 1 \end{vmatrix}, \quad d = -\begin{vmatrix} x_1^2 + y_1^2 & y_1 & 1 \\ x_2^2 + y_2^2 & y_2 & 1 \\ x_3^2 + y_3^2 & y_3 & 1 \end{vmatrix}, \quad e = \begin{vmatrix} x_1^2 + y_1^2 & x_1 & 1 \\ x_2^2 + y_2^2 & x_2 & 1 \\ x_3^2 + y_3^2 & x_3 & 1 \end{vmatrix},$$

and

$$f = -\begin{vmatrix} x_1^2 + y_1^2 & x_1 & y_1 \\ x_2^2 + y_2^2 & x_2 & y_2 \\ x_3^2 + y_3^2 & x_3 & y_3 \end{vmatrix}.$$

Now we may define a similarity mapping which maps $z_1, z_2, z_3 = a, b, 0$ onto the unit circle by

$$w(z) = (z - z_0)/r,$$

where $z_0 = x_0 + iy_0$ and r is as above.

2.7. Mapping unbounded onto bounded domains. The transformation $z \mapsto z/|z|^2$ maps the complement of the closed unit disk onto the unit disk. This transformation is an anticonformal mapping and it maps the complement of a polygonal quadrilateral with vertices a, b, c, d with $|b| = |c| = |d| = 1$ onto a bounded domain, bounded by four circular arcs. Note that the points b, c, d remain invariant under this transformation. See Figure 1.

2.8. The Dirichlét-Neumann problem. The following problem is known as the *Dirichlét-Neumann problem*. Let D be a region in the complex plane whose boundary ∂D consists of a finite number of regular Jordan curves, so that at every point, except possibly at finitely many points, of the boundary a normal is defined. Let $\partial D = A \cup B$ where A, B both are unions of Jordan arcs. Let ψ_A, ψ_B be a real-valued continuous functions defined on A, B , respectively. Find a function u satisfying the following conditions:

- (1) u is continuous and differentiable in \overline{D} .
- (2) $u(t) = \psi_A(t)$, for all $t \in A$.
- (3) If $\partial/\partial n$ denotes differentiation in the direction of the exterior normal, then

$$\frac{\partial}{\partial n} u(t) = \psi_B(t), \quad \text{for all } t \in B.$$

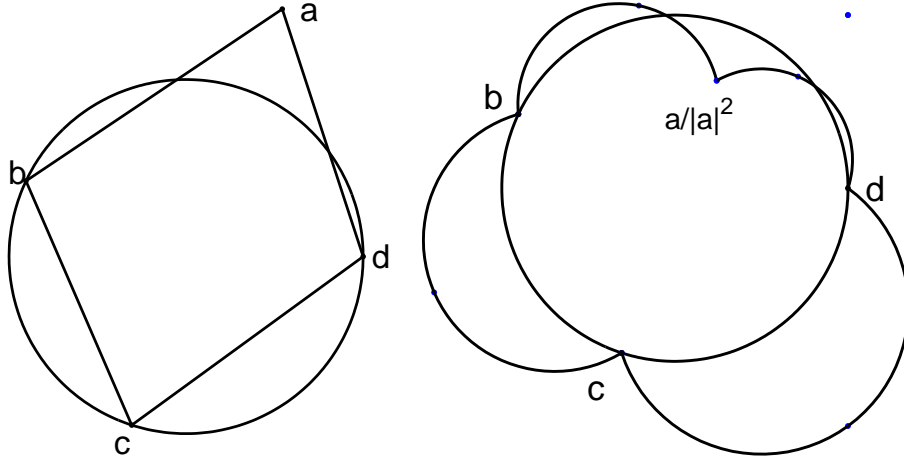


FIGURE 1. Polygonal quadrilateral before (left) and after (right) the inversion transformation $z \mapsto z/|z|^2$. Note that the points b, c, d on the unit circle remain invariant.

2.9. Modulus of a quadrilateral and Dirichlét integrals. One can express the modulus of a quadrilateral $(D; z_1, z_2, z_3, z_4)$ in terms of the solution of the Dirichlét-Neumann problem as follows. Let $\gamma_j, j = 1, 2, 3, 4$ be the arcs of ∂D between (z_4, z_1) , (z_1, z_2) , (z_2, z_3) , (z_3, z_4) , respectively. If u is the (unique) harmonic solution of the Dirichlét-Neumann problem with boundary values of u equal to 0 on γ_2 , equal to 1 on γ_4 and with $\partial u / \partial n = 0$ on $\gamma_1 \cup \gamma_3$, then by [1, p. 65/Thm 4.5]:

$$(2.10) \quad \mathbf{M}(D; z_1, z_2, z_3, z_4) = \iint_D |\nabla u|^2 dx dy.$$

2.11. The reciprocal identity. Given a quadrilateral $Q = (D; z_1, z_2, z_3, z_4)$ we call sometimes $\tilde{Q} = (D; z_2, z_3, z_4, z_1)$ the conjugate quadrilateral. It is a simple basic fact that

$$(2.12) \quad \mathbf{M}(Q)\mathbf{M}(\tilde{Q}) = 1.$$

It was suggested in [15] and [14] that the quantity

$$(2.13) \quad r(Q) = |\mathbf{M}(Q)\mathbf{M}(\tilde{Q}) - 1|$$

might serve as a useful error characteristic. We will continue to use this also in our work.

3. THE hp -FEM METHOD

In this section we describe the high-order p -, and hp -finite element methods. The paper of Babuška and Suri [6] gives an accessible overview of the method. For a more detailed exposition we refer to Schwab [24], and for those familiar with engineering approach the book by Szabo and Babuška [25] is recommended. The presentation here follows closely earlier work by the authors [14].

For the applications considered in this paper, any finite element computation requires at least the choice of the following.

- (1) Initial discretization of the domain. In 2D each discretization or mesh divides the domain into elements, plane regions with piecewise smooth boundaries. These are usually either triangles or quadrilaterals.
- (2) Refinement strategy. The choice of the refinement strategy is connected to choosing the finite element method (FEM): mesh refinement (h -method), elementwise polynomial order (p -method), or both (hp -method). The unknowns or degrees of freedom are the coefficients of the chosen shape functions. In the h -version, the shape functions are such that the coefficients are also values of the solution at specified locations of the discretization of the computational domain, that is, the nodes of the mesh. In the p -method, the shape functions are polynomials that are associated with topological entities of the elements, nodes, sides, and interior. Thus, in addition to increasing accuracy through refining the mesh, we have an additional refinement parameter, the polynomial degree p .

Refinement strategies can be based on *a priori* and *a posteriori* error estimates. In all cases considered here, sufficient *a priori* knowledge of the singularities exist for the construction of the properly graded meshes. All modifications of the refinement strategy always imply recomputing of the entire solution.

What makes the exterior modulus problem especially interesting from the finite element point of view is the natural appearance of computational domains with cusps. Our experience shows that the standard geometric grading is adequate also in this class of problems. In the cases when reference solutions are not available, we rely on the reciprocal identity as our fundamental quality measure.

Let us next define a p -type quadrilateral element. The construction of triangles is similar and can be found from the references given above.

3.1. Shape functions. Many different selections of shape functions are possible. We follow Szabo and Babuška [25] and present the so-called hierarchic shape functions.

Legendre polynomials of degree n can be defined using a recursion formula

$$(3.1) \quad (n+1)P_{n+1}(x) - (2n+1)xP_n(x) + nP_{n-1}(x) = 0, \quad P_0(x) = 1.$$

The derivatives can similarly be computed using a recursion

$$(3.2) \quad (1-x^2)P'_n(x) = -nP_n(x) + nP_{n-1}(x).$$

For our purposes the central polynomials are the integrated Legendre polynomials for $x \in [-1, 1]$,

$$(3.3) \quad \phi_n(\xi) = \sqrt{\frac{2n-1}{2}} \int_{-1}^{\xi} P_{n-1}(t) dt, \quad n = 2, 3, \dots,$$

which can be rewritten as linear combinations of Legendre polynomials

$$(3.4) \quad \phi_n(\xi) = \frac{1}{\sqrt{2(2n-1)}} (P_n(\xi) - P_{n-2}(\xi)), \quad n = 2, 3, \dots$$

The normalizing coefficients are chosen so that

$$(3.5) \quad \int_{-1}^1 \frac{d\phi_i(\xi)}{d\xi} \frac{d\phi_j(\xi)}{d\xi} d\xi = \delta_{ij}, \quad i, j \geq 2.$$

We can now define the shape functions for a quadrilateral reference element over the domain $[-1, 1] \times [-1, 1]$. The shape functions are divided into three categories: nodal shape functions, side modes, and internal modes.

3.2. Nodal shape functions. There are four nodal shape functions:

$$\begin{aligned} N_1(\xi, \eta) &= \frac{1}{4}(1 - \xi)(1 - \eta), \\ N_2(\xi, \eta) &= \frac{1}{4}(1 + \xi)(1 - \eta), \\ N_3(\xi, \eta) &= \frac{1}{4}(1 + \xi)(1 + \eta), \\ N_4(\xi, \eta) &= \frac{1}{4}(1 - \xi)(1 + \eta). \end{aligned}$$

Taken alone, these shapes define the standard four-node quadrilateral finite element.

3.3. Side shape functions. There are $4(p-1)$ side modes associated with the sides of a quadrilateral ($p \geq 2$):

$$\begin{aligned} N_i^{(1)}(\xi, \eta) &= \frac{1}{2}(1 - \eta)\phi_i(\xi), \quad i = 2, \dots, p, \\ N_i^{(2)}(\xi, \eta) &= \frac{1}{2}(1 + \xi)\phi_i(\eta), \quad i = 2, \dots, p, \\ N_i^{(3)}(\xi, \eta) &= \frac{1}{2}(1 + \eta)\phi_i(\eta), \quad i = 2, \dots, p, \\ N_i^{(4)}(\xi, \eta) &= \frac{1}{2}(1 - \xi)\phi_i(\xi), \quad i = 2, \dots, p. \end{aligned}$$

3.4. Internal shape functions. For the internal modes we have two options. The so-called trunk space has $(p-2)(p-3)/2$ shapes

$$(3.6) \quad N_{i,j}^0(\xi, \eta) = \phi_i(\xi)\phi_j(\eta), \quad i, j \geq 2, \quad i + j = 4, 5, \dots, p,$$

whereas the full space has $(p-1)(p-1)$ shapes

$$(3.7) \quad N_{i,j}^0(\xi, \eta) = \phi_i(\xi)\phi_j(\eta), \quad i = 2, \dots, p, \quad j = 2, \dots, p.$$

In this paper we always use the full space. The internal shape functions are often referred to as bubble-functions.

3.5. Parity problem. The Legendre polynomials have the property $P_n(-x) = (-1)^n P_n(x)$. In 2D all internal edges of the mesh are shared by two different elements. We must ensure that each edge has the same global parametrization in both elements. This additional book-keeping is not necessary in the standard h -FEM.

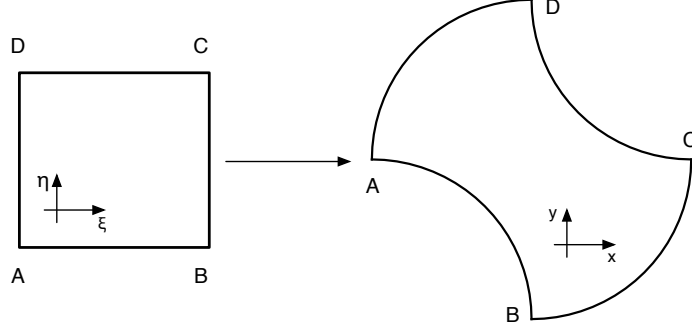


FIGURE 2. Curved boundary mapping.

3.6. Domains with curved boundaries. It is important to represent curved boundary segments accurately. The linear blending function method of Gordon and Hall [12] is our choice for this purpose.

In the general case all sides of an element can be curved as in Figure 2. We assume that every side is parametrized as follows:

$$(3.8) \quad x = x_i(t), \quad y = y_i(t), \quad -1 \leq t \leq 1, \quad i = 1, \dots, \text{number of sides}$$

Using capital letters as coordinates of the corner points, (X_i, Y_i) , we can write the mapping for the global x -coordinates of a quadrilateral as

$$(3.9) \quad \begin{aligned} x = & \frac{1}{2}(1 - \eta)x_1(\xi) + \frac{1}{2}(1 + \xi)x_2(\eta) + \frac{1}{2}(1 + \eta)x_3(\xi) + \frac{1}{2}(1 - \xi)x_4(\eta) \\ & - \frac{1}{4}(1 - \xi)(1 - \eta)X_1 - \frac{1}{4}(1 + \xi)(1 + \eta)X_2 - \frac{1}{4}(1 + \xi)(1 + \eta)X_3 \\ & - \frac{1}{4}(1 - \xi)(1 + \eta)X_4, \end{aligned}$$

and symmetrically for the y -coordinate. Note, that if the side parametrizations represent straight edges, the mapping simplifies to the standard bilinear mapping of quadrilaterals.

In the following we always use exact representation of the geometry which implies that in the ensuing mesh grading process no approximation of geometry is necessary.

3.7. Proper grading of the meshes. For a certain class of problems it can be shown that if the mesh and the elemental degrees have been set optimally, we can obtain *exponential convergence*. A geometric mesh is such that each successive layer of elements changes in size with some *geometric scaling factor* α , toward some point of interest. In this case, the points of interest are always corner points.

The following theorem is due to Babuška and Guo [4]. Note that construction of appropriate spaces is technical. For rigorous treatment of the theory involved see Schwab [24], Babuška and Guo [5] and references therein.

Theorem 1. Let $\Omega \subset \mathbb{R}^2$ be a polygon, v the FEM-solution, and let the weak solution u_0 be in a suitable countably normed space where the derivatives of arbitrarily high

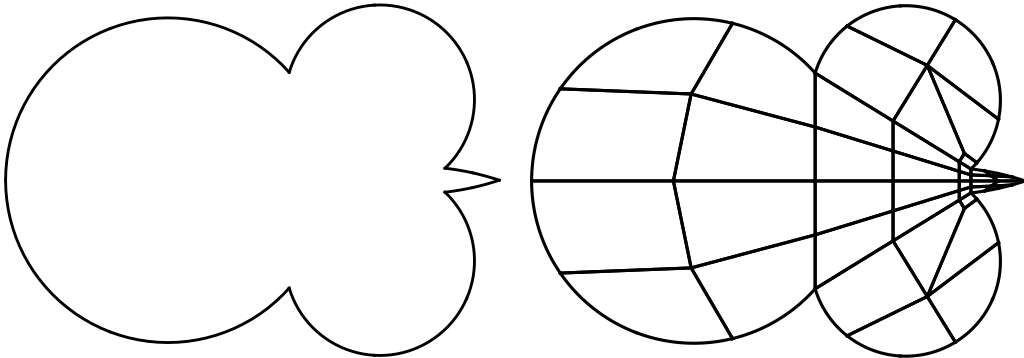


FIGURE 3. A sample geometry and the corresponding initial mesh. Note that the three-element -rule is satisfied at every corner.

order are controlled. Then

$$\inf_v \|u_0 - v\|_{H^1(\Omega)} \leq C \exp(-b\sqrt[3]{N}),$$

where C and b are independent of N , the number of degrees of freedom. Here v is computed on a proper geometric mesh, where the orders of individual elements depend on their originating layer, such that the highest layers have the smallest orders.

The result also holds for constant polynomial degree distribution.

Let us denote the number of the highest layer with ν , *the nesting level*. Using this notation we refer to geometric meshes as (α, ν) -meshes.

3.8. Generating geometric meshes. We use the following two-phase algorithm where triangles can be replaced by quadrilaterals or a mixture of both:

- (1) Generate an initial mesh (triangulation) where the corners are isolated with a fixed number of triangles depending on the interior angle, θ so that the refinements can be carried out independently:
 - (a) $\theta \leq \pi/2$: one triangle,
 - (b) $\pi/2 < \theta \leq \pi$: two triangles, and
 - (c) $\pi < \theta$: three triangles.
- (2) Every triangle attached to a corner is replaced by a refinement, where the edges incident to the corner are split as specified by the scaling factor α . This process is repeated recursively until the desired nesting level ν is reached. Note that the mesh may include quadrilaterals after refinement.

Since the choice of the initial mesh affects strongly the refinement process, it is advisable to test with different choices. Naturally, one would want the initial mesh to be minimal, that is, having the smallest possible number of elements yet providing support for the refinement. This is why initial meshes are sometimes referred to as minimal meshes.

In Figure 3 a challenging example is shown. In this case the large variation of the edge lengths is addressed by adding a refinement step to the construction of the

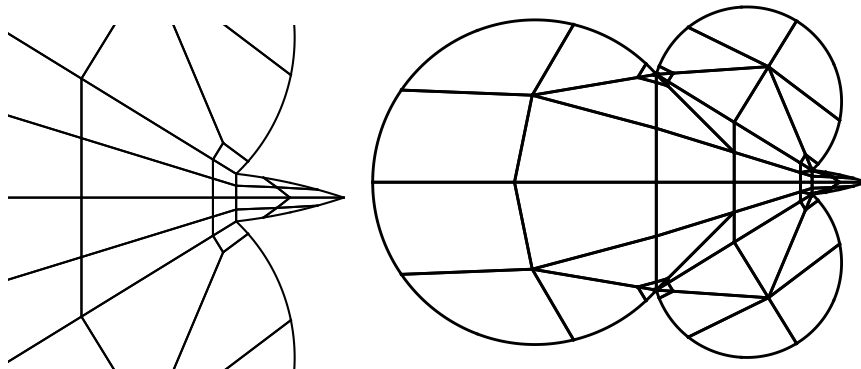


FIGURE 4. A detail of the initial mesh and the final $(0.15, 14)$ -mesh used in the actual computation.

initial mesh. A detail of the initial mesh is given in Figure 4 along with the final mesh.

3.9. p -Distribution. If so desired, the polynomial degree can be varied over the mesh. In Theorem 1 the degrees are connected to the refinement layers. At every step in the mesh grading process a new layer of elements is created. Those elements belonging to the final layer are assigned the lowest polynomial degree.

This layer representation can always be recovered by considering graph-distances in the graph of the dual mesh, that is, in the graph where the elements are vertices and edges indicated a shared edge in the actual mesh. Elements adjacent to points of singularity are considered equivalent to those created at the final step.

4. THE CASE OF A RECTANGLE

The first tests with the hp -FEM software were made for the case of the exterior modulus of a rectangle and checked against the Duren-Pfaltzgraff formula (2.5). For a convenient parametrization of the computation, the vertices of the rectangle were chosen to be the points $1, e^{it}, -1, -e^{it}, t \in (0, \pi/2]$ of the unit circle. In this case, the "interior" modulus of the rectangle is $\tan(t/2)$. It is equal to the modulus of the family of curves joining the sides $[1, e^{it}]$ and $[-1, -e^{it}]$ and lying in the interior of the rectangle. The formula (2.5) now gives the corresponding exterior modulus as

$$\frac{\mathcal{K}'(k)}{2\mathcal{K}(k)}, \quad k = \psi^{-1}\left(\frac{1}{\tan(t/2)}\right).$$

For the computation, we carried out the inversion $z \mapsto 1/\bar{z}$ in the unit circle which keep all the points of the unit circle fixed and transforms the exterior modulus problem for the rectangle to the "interior" modulus problem of a plane domain bounded by four circular arcs, see Figure 5. These circular arcs are the images of the sides of the rectangle under the inversion. The results turned out to be quite accurate, with a typical relative error of the order 10^{-10} .

TABLE 1. Exact values of the moduli of $Q(1, e^{it}, -1, -e^{it})$ given by (2.5) and the errors of computational results of the hp -method, $p = 20$, the AFEM method and the SC Toolbox. The errors are obtained by comparing with the exact formula (2.5). The errors are given as $\lceil \log_{10} |\text{error}| \rceil$.

k	exact($t = k\pi/12$)	Error[hpFEM]	Error[AFEM]	Error[SCT]
1	1.50290233467	-9	-6	-9
2	1.31044063554	-9	-6	-9
3	1.20035166917	-9	-6	-10
4	1.12114255114	-10	-6	-9
5	1.05681535228	-10	-6	-13
6	1.	-10	-6	-15

5. SIDE SLIDING CONJECTURE

In this section we will study side sliding problem.

5.1. The side sliding problem. Consider the problem of finding the minimal exterior modulus of the polygonal quadrilateral with vertices $0, 1, a = t + ih, b = t - s + ih$ when $h, s > 0$ are fixed and t varies. We consider the question of computing the modulus of the family Γ of curves joining the opposite sides $[1, a]$ and $[b, 0]$ outside the quadrilateral. Our first step is to reduce the problem to an equivalent problem such that three of the points are on the unit circle. Note that this setting is valid only if z_0 is inside the quadrilateral. Indeed, for every choice of h and s this condition defines an upper limit for the value of t .

5.2. Side sliding conjecture. The least value of the exterior modulus is attained when $t = (1 + s)/2$. For $t \leq (1 + s)/2$ the modulus is a decreasing function of t .

5.3. Numerical experiments on side sliding conjecture. In Figure 7 we show a graph of the exterior module as a function of the parameter $t \in [0.5, 2.5]$, when $h = 1, s = 2$. The computation was carried out with SC Toolbox, hp -FEM, and AFEM and for the range of computed values, the respective graphs coincide. For the SC Toolbox and the hp -FEM the reciprocal estimate for the error was smaller than 10^{-8} and for AFEM 10^{-5} .

6. THE CASE OF A SYMMETRIC HEXAGON

Suppose that $Q(a, b, 0, 1)$ is a quadrilateral in the upper half plane. Then the closed polygonal line $a, b, 0, \bar{b}, \bar{a}, 1, a$ defines a hexagon $H = Q \cup \bar{Q}$ symmetric with respect to the real axis. Map the complement of H onto $\mathbb{C} \setminus \{-1 - t, 1 + t\}$ by a conformal map h such that $h(0) = -1 - t, h(b) = h(\bar{b}) = -1, h(a) = h(\bar{a}) = 1, h(1) = 1 + t$ where $t > 0$ depends on the point configuration $a, b, 0, 1$. It is clear by symmetry that

$$(6.1) \quad 2M(\Delta^+) = M(\Delta)$$

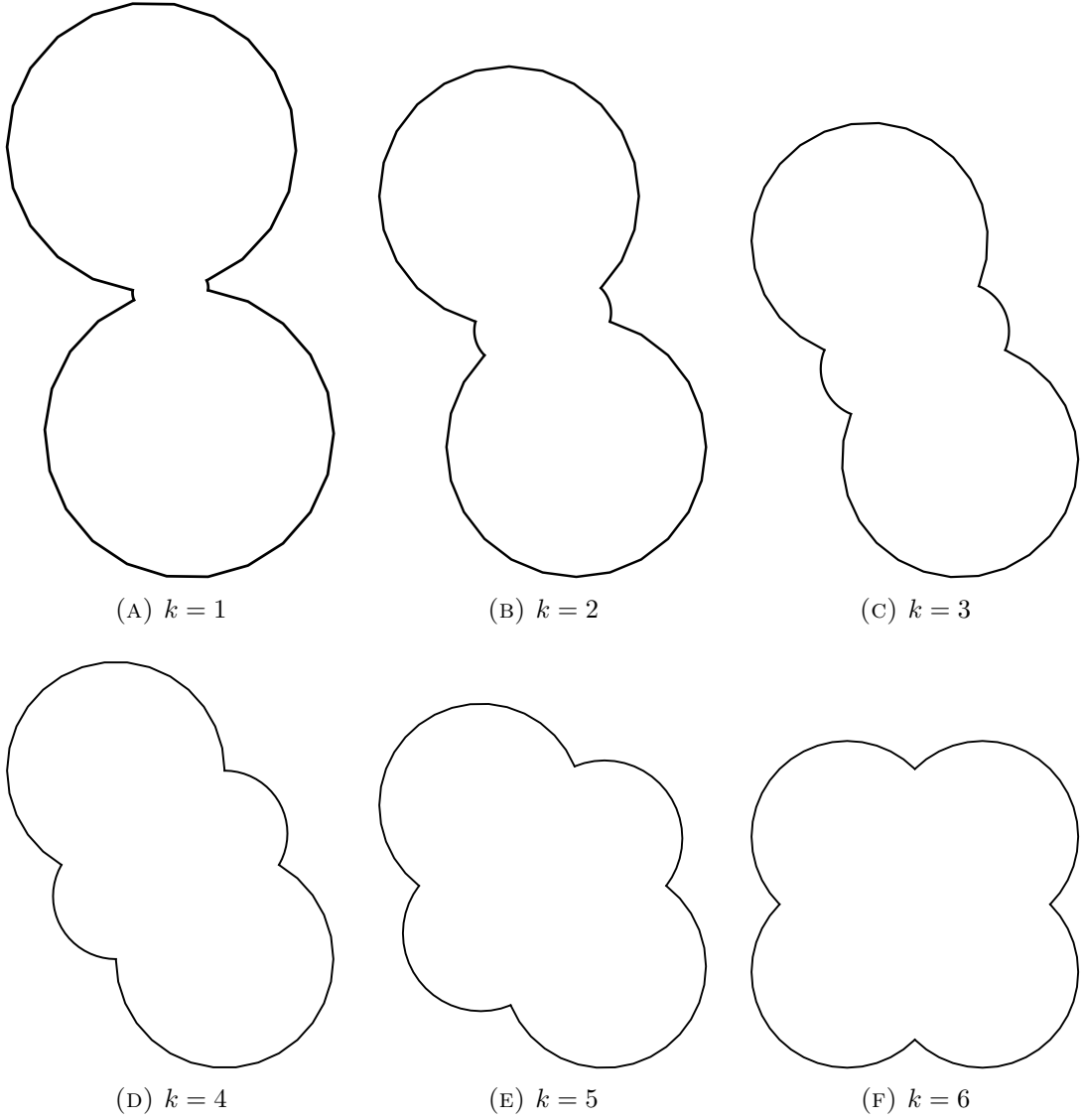


FIGURE 5. Circular arc domains used for the hp -FEM computations of the values in Table 1. The scale varies from picture to picture.

where

$$\Delta = \Delta([-1-t, -1], [1, 1+t]; \mathbb{C}) \text{ and } \Delta^+ = \Delta([-1-t, -1], [1, 1+t]; \{z : \text{Im } z > 0\}).$$

Because of the conformal invariance of the modulus we also have

$$(6.2) \quad 2\mathbf{M}(h^{-1}(\Delta^+)) = \mathbf{M}(h^{-1}(\Delta)).$$

Applying this formula with (2.5) we see that

$$(6.3) \quad \mathbf{M}(\Gamma_+) = \frac{\mathcal{K}'(k)}{4\mathcal{K}(k)}, \quad k = \psi^{-1}\left(\frac{1}{2h}\right),$$

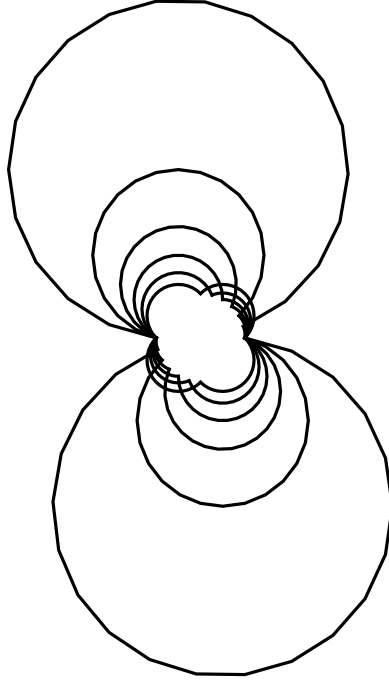
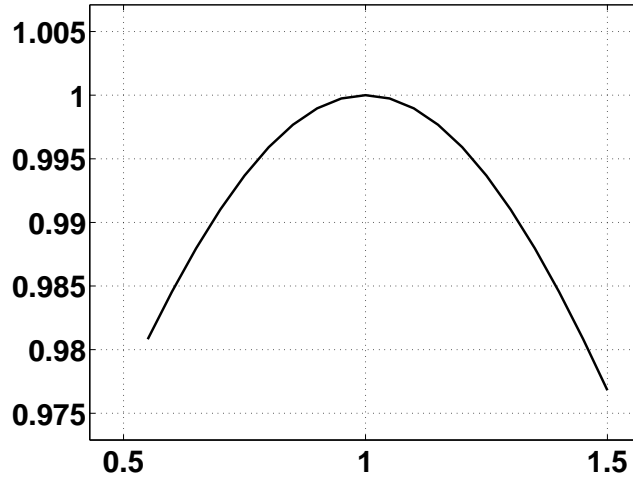


FIGURE 6. The circular arc domains of Figure 5 in the same scale.

FIGURE 7. Side Sliding Conjecture: Dependence of the exterior modulus on parameter t with $h = 1, s = 1$. Maximum is reached at $t = (1 + s)/2 = 1$, as predicted by the conjecture.

where for $h > 0$,

$$(6.4) \quad \Gamma_+ = \Delta([0, ih], [1, 1 + ih]; \mathbb{C}_+ \setminus [0, 1] \times [0, h]).$$

This formula can be checked by using the SC Toolbox to construct the above conformal mapping h . The tests we carried out for $h = 0.2, 0.3, 0.4$ and 0.5 . In these cases the reciprocal estimate for error was smaller than 10^{-9} .

7. GENERAL QUADRILATERAL

The exterior modulus of the quadrilateral Q with vertices a, b, c, d is considered in this section, i.e., we compute

$$\iint_Q |\nabla u|^2 dx dy$$

over the complement of the quadrilateral when u is the solution of the Laplace equation in the complement of the quadrilateral with Dirichlet values 1 and 0 on the sides $[b, c]$ and $[d, a]$, respectively, and the Neumann value 0 on the sides $[a, b]$ and $[c, d]$. Here we allow the boundary of the quadrilateral ∂Q , be a parametrized curve $\gamma(t)$, $t \in [-1, 1]$.

In Figure 8 an overview of the standard FEM approach is given. Using higher-order elements one can stretch the domain without introducing significant number of elements. Singularities at the corner point must be accounted for in the grading of the mesh. Since both the circle and the square cases are symmetric, the exterior modulus is exactly 1, and furthermore the potential value at infinity or the far-field value is exactly $1/2$.

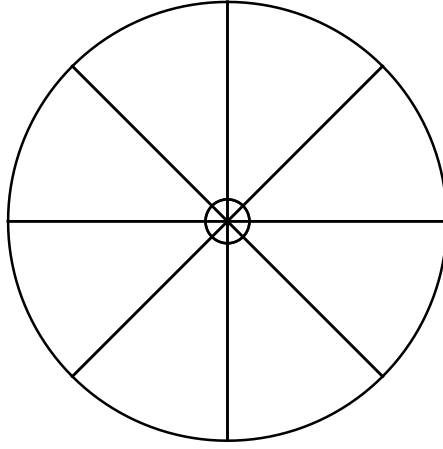
In Tables 2, 3, and 6 results on two polygonal quadrilaterals

- Quadrilateral A: $\{0, 1, (28/25, 69/50), (-19/25, 21/25)\}$,
- Quadrilateral B: $\{0, 1, (42/25, 4), (-3/25, 21/25)\}$,

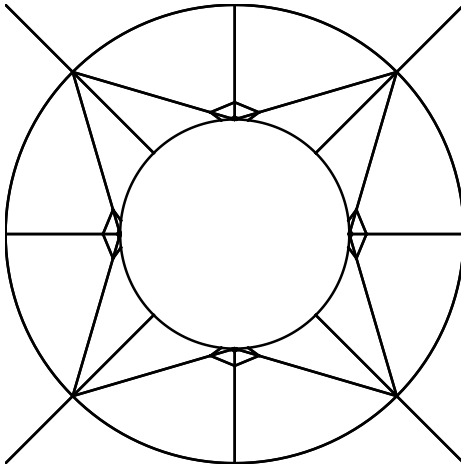
are presented. The exterior modulus has been computed using three methods as an equivalent interior modulus problem, and also in truncated domain. In the interior case, both SC Toolbox and hp -FEM give similar results, but AFEM in its standard setting does not reach the desired accuracy. This is probably due to the adaptive scheme failing in the presence of cusps in the domain. Tables 2 and 3 indicate that large exterior angles are the most significant source of errors in the FEM solutions, as expected. In the rather benign setting of the Quadrilateral A, SC Toolbox and both the internal and external hp -FEM versions have the same accuracy, but in the case of Quadrilateral B, we see gradual loss of accuracy in the FEM solutions.

Finally, we consider two flower domains, that is, quadrilateral domains with the boundary $\gamma(t) = r(t)e^{it}$, $r(t) = 4/5 + (1/5)\cos(n\pi t)$ and corners at $t = -1, -1/4, 0, 1/2$. For the Quadrilateral C we choose $n = 4$ and for D we choose $n = 8$. These domains have the useful property that the exterior problem can easily be converted to a corresponding interior problem of the domain with boundary $1/\overline{\gamma(t)}$. Since these domains cannot be handled using the SC Toolbox, we take the interior solution as the reference. Tables 4 and 5 show that we can obtain results of high accuracy also in traditionally challenging domains.

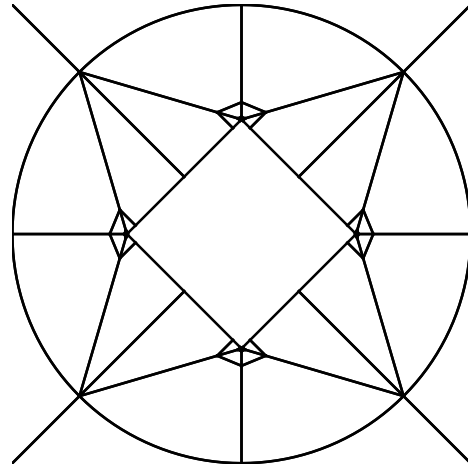
It turns out that besides the actual value of the exterior modulus one can also determine the value of the far-field potential. Either one can determine the value of the potential at the reflection point of the interior problem, i.e., at the origin, or simply evaluate the solution of the exterior problem at the farthest point. Remarkably, the truncated domain results agree well with the (theoretically) exact results of the equivalent inner modulus problems (Table 6). In Figures 9–12 we show comparisons of the interior and exterior potential fields. For the two polygonal quadrilaterals, the corresponding contour lines and the location of the origin in the interior case



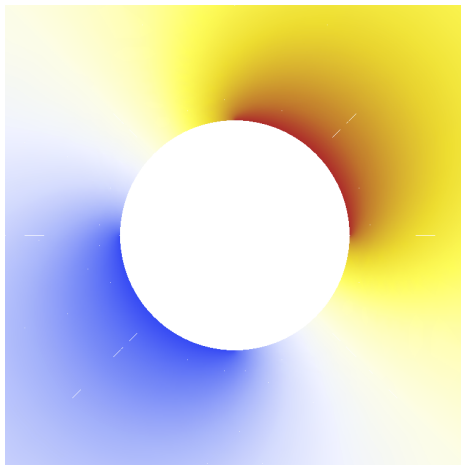
(A) Exterior domain
with radius > 1000000 .



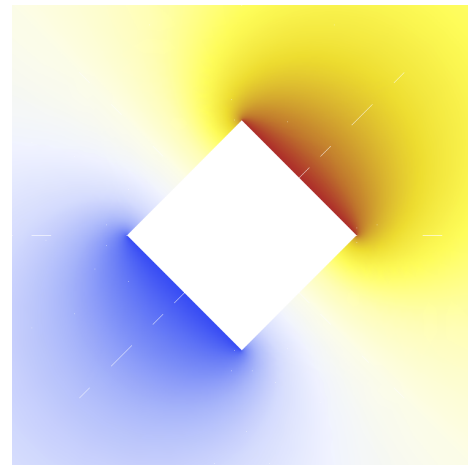
(B) Zoom of the mesh
in the case of a circle.



(C) Zoom of the mesh
in the case of a square.



(D) Zoom of the po-
tential in the case of a
circle. Reciprocal error
 $\sim 8.8 \cdot 10^{-10}$



(E) Zoom of the po-
tential in the case of a
square. Reciprocal er-
ror $\sim 6.3 \cdot 10^{-10}$

FIGURE 8. Exterior modulus over the exterior domain.

Method	Exterior Modulus	Error (2.13)	Relative Error
SC Toolbox	0.9923416323	-9	—
AFEM	0.9923500126	-4	-5
hp -FEM (Interior)	0.9923416332	-9	-9
hp -FEM (Exterior)	0.9923416332	-9	-9

TABLE 2. Quadrilateral A: $\{0, 1, (28/25, 69/50), (-19/25, 21/25)\}$. The values obtained with SC Toolbox are used as reference. The errors are given as $\lceil \log_{10} |\text{error}| \rceil$.

Method	Exterior Modulus	Error (2.13)	Relative Error
SC Toolbox	0.9592571721	-9	—
AFEM	0.9593012739	-4	-4
hp -FEM (Interior)	0.9592571731	-8	-8
hp -FEM (Exterior)	0.9592572007	-7	-7

TABLE 3. Quadrilateral B: $\{0, 1, (42/25, 4), (-3/25, 21/25)\}$. The values obtained with SC Toolbox are used as reference. The errors are given as $\lceil \log_{10} |\text{error}| \rceil$.

Method	Exterior Modulus	Error (2.13)	Relative Error
hp -FEM (Interior)	0.8196441884805177	-14	—
hp -FEM (Exterior)	0.8196441926483611	-8	-8

TABLE 4. Quadrilateral C: $\gamma(t) = r(t)e^{it}$, $r(t) = 4/5 + (1/5)\cos(4\pi t)$ and corners at $t = -1, -1/4, 0, 1/2$. The values obtained with hp -FEM (Interior) are used as reference. The errors are given as $\lceil \log_{10} |\text{error}| \rceil$.

Method	Exterior Modulus	Error (2.13)	Relative Error
hp -FEM (Interior)	0.9122187602015264	-10	—
hp -FEM (Exterior)	0.9122187628550672	-8	-8

TABLE 5. Quadrilateral D: $\gamma(t) = r(t)e^{it}$, $r(t) = 4/5 + (1/5)\cos(8\pi t)$ and corners at $t = -1, -1/4, 0, 1/2$. The values obtained with hp -FEM (Interior) are used as reference. The errors are given as $\lceil \log_{10} |\text{error}| \rceil$.

are indicated. In the general case, prediction of the far-field value based solely on geometric arguments is an open problem.

We note, that for both Quadrilateral C and D, the interior and exterior capacities are equal. This invariance is new and has not been reported in the literature before. It is crucial that the four corners are chosen from extremal points, that is, local minima and maxima of the radius.

Quadrilateral	hp -FEM (Interior)	hp -FEM (Exterior)	Relative Error
A	0.5281867366243582	0.5281867468410989	-7
B	0.6659476737428786	0.6659476800244547	-8
C	0.5873283399651075	0.5873283469398137	-7
D	0.5398927341965689	0.5398927414203410	-7

TABLE 6. Comparison of the computed values of the potential at infinity. The errors are given as $\lceil \log_{10} |\text{error}| \rceil$.

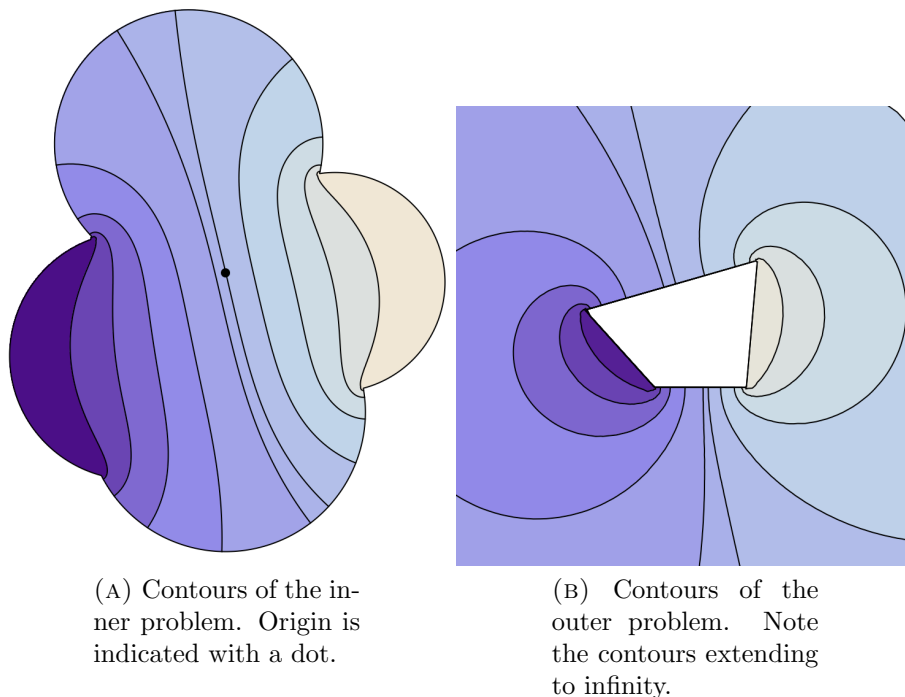


FIGURE 9. Quadrilateral A: Correspondence of the potential contours between the inner (A) and outer (B) solutions. Shown are the potential levels $u(z) = 0, 1/10, \dots, 1$, and $u(0)$. Corresponding contours can be identified by matching the shadings of the regions in between.

8. CONCLUSIONS

In this study we have shown that three different algorithms, AFEM, SC Toolbox and hp -FEM, can all be effectively used for computation of the exterior modulus of a bounded quadrilateral. The problem is first reduced to a Dirichlet-Neumann problem for the Laplace equation. In our earlier paper [14] we introduced the reciprocal identity as an error estimate for the inner modulus computation and here we demonstrate that the same method applies to error estimation for the exterior modulus as well. As far as we know, there are very few numerical or theoretical results on the exterior modulus in the literature. We compare our numerical results to the

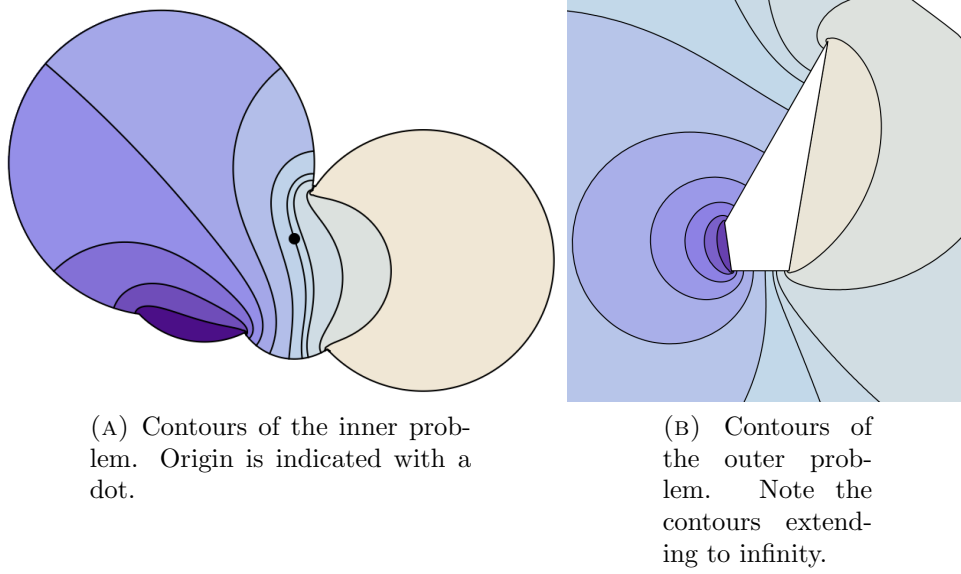


FIGURE 10. Quadrilateral B: Correspondence of the potential contours between the inner (A) and outer (B) solutions. Shown are the potential levels $u(z) = 0, 1/10, \dots, 1$, and $u(0)$. Corresponding contours can be identified by matching the shadings of the regions in between.

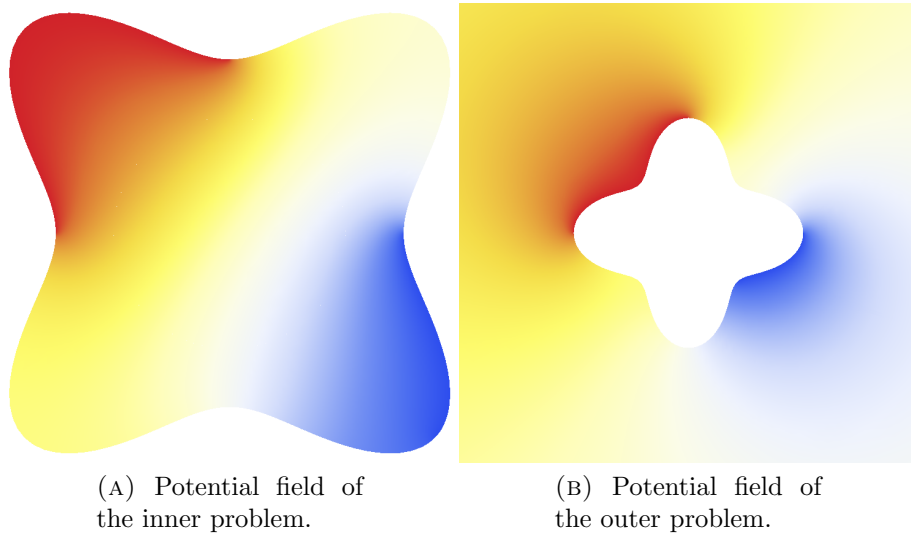


FIGURE 11. Quadrilateral C: The potential field of the inner (A) and outer (B) solutions.

Duren-Pfaltzgraff formula for the exterior modulus of a rectangle and observe that our results agree with it, within the limits provided by the reciprocal error estimate.

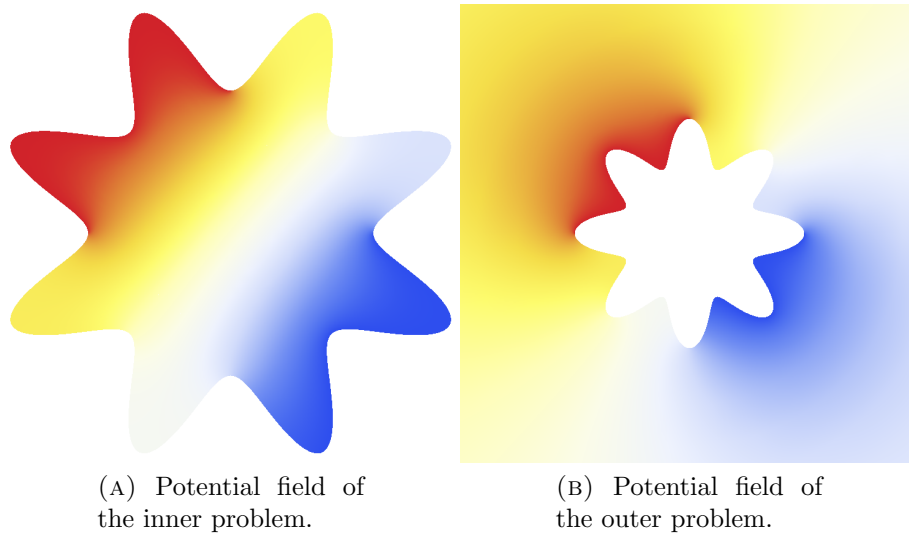


FIGURE 12. Quadrilateral D: The potential field of the inner (A) and outer (B) solutions.

A problem of independent interest is the value of the potential function at infinity. We study this problem for the exterior modulus of a polygonal quadrilateral and solve it by mapping the exterior domain onto a bounded domain by inversion and then computing the value of the potential function of the corresponding interior modulus problem at the image point of the point at infinity.

We anticipate that the problem of exterior modulus could also be studied using integral equation methods.

Acknowledgement. The research of Matti Vuorinen was supported by the Academy of Finland, Project 2600066611.

REFERENCES

- [1] L.V. AHLFORS, *Conformal invariants: topics in geometric function theory*. McGraw-Hill Book Co., 1973.
- [2] G.D. ANDERSON, M.K. VAMANAMURTHY and M. VUORINEN, *Conformal invariants, inequalities and quasiconformal mappings*, Wiley-Interscience, 1997.
- [3] S. AXLER, P. BOURDON, and W. RAMEY, *Harmonic Function Theory*, Graduate Texts in Mathematics, 2nd ed., Springer, 2001.
- [4] I. BABUŠKA and B. GUO, *Regularity of the solutions of elliptic problems with piecewise analytical data, parts I and II*, SIAM J. Math. Anal., 19, (1988), 172–203 and 20, (1989), 763–781.
- [5] I. BABUŠKA and B. GUO, *Approximation properties of the hp -version of the finite element method*, Comp. Meth. Appl. Mech. Engr., 133, (1996), 319–346.
- [6] I. BABUŠKA and M. SURI, *The P and H - P versions of the finite element method, basic principles and properties*, SIAM Review 36 (1994), 578–632.
- [7] D. BETSAKOS, K. SAMUELSSON and M. VUORINEN, *The computation of capacity of planar condensers*, Publ. Inst. Math. 75 (89) (2004), 233–252.
- [8] W.G. BICKLEY, *Two-dimensional potential problems for the space outside a rectangle*, Proc. Lond. Math. Soc., Ser. 2, (37) (1932), 82–105.

- [9] T.A. DRISCOLL, *Schwarz-Christoffel toolbox for MATLAB*, <http://www.math.udel.edu/~driscoll/SC/>
- [10] T.A. DRISCOLL and L.N. TREFETHEN, *Schwarz-Christoffel mapping*. Cambridge Monographs on Applied and Computational Mathematics, 8. Cambridge University Press, Cambridge, 2002.
- [11] P. DUREN and J. PFALTZGRAFF, *Robin capacity and extremal length*. J. Math. Anal. Appl. 179 (1993), no. 1, 110–119.
- [12] W.J. GORDON and C.A. HALL, *Transfinite element methods: blending function interpolation over arbitrary curved element domains*, Numer. Math. 21 (1973), pp. 109–129.
- [13] H. HAKULA, T. QUACH and A. RASILA, *Conjugate Function Method for Numerical Conformal Mappings*. arXiv:1103.4930 [math.NA].
- [14] H. HAKULA, A. RASILA, and M. VUORINEN, *On moduli of rings and quadrilaterals: algorithms and experiments*. SIAM J. Sci. Comput. 33 (2011), pp. 279–302 (24 pages), DOI: 10.1137/090763603, arXiv:0906.1261 [math.NA].
- [15] V. HEIKKALA, M.K. VAMANAMURTHY and M. VUORINEN, *Generalized elliptic integrals*, Comput. Methods Funct. Theory 9 (2009), 75–109. arXiv math.CA/0701436.
- [16] P. HENRICI, *Applied and Computational Complex Analysis*, vol. III, Wiley-Interscience, 1986.
- [17] P. HOUGH, *CONFPACK*. Available from Netlib collection of mathematical software. <http://www.netlib.org/conformal/>
- [18] R. KÜHNAU, *The conformal module of quadrilaterals and of rings*, In: Handbook of Complex Analysis: Geometric Function Theory, (ed. by R. Kühnau) Vol. 2, North Holland/Elsevier, Amsterdam, 99–129, 2005.
- [19] P.K. KYTHE, *Computational conformal mapping*, Birkhäuser, 1998.
- [20] O. LEHTO and K.I. VIRTANEN, *Quasiconformal mappings in the plane*, 2nd edition, Springer, Berlin, 1973.
- [21] F.W.J. OLVER, D.W. LOZIER, R.F. BOISVERT, and C.W. CLARK, EDS., *NIST Handbook of Mathematical Functions*, Cambridge Univ. Press, Cambridge, 2010. <http://dlmf.nist.gov>.
- [22] N. PAPAMICHAEL and N.S. STYLIANOPOULOS, *Numerical Conformal Mapping: Domain Decomposition and the Mapping of Quadrilaterals*, World Scientific, 2010.
- [23] R. SCHINZINGER and P. LAURA, *Conformal Mapping: Methods and Applications*, Elsevier, Amsterdam 1991.
- [24] CH. SCHWAB, *p- and hp-Finite Element Methods*, Oxford University Press, 1998.
- [25] B. SZABO and I. BABUŠKA, *Finite Element Analysis*, Wiley, 1991.
- [26] L.N. TREFETHEN, *Numerical computation of the Schwarz-Christoffel transformation*. SIAM J. Sci. Statist. Comput. 1 (1980), no. 1, 82–102.
- [27] L.N. TREFETHEN and T.A. DRISCOLL, *Schwarz-Christoffel mapping in the computer era*. Proceedings of the International Congress of Mathematicians, Vol. III (Berlin, 1998). Doc. Math. 1998, Extra Vol. III, 533–542.

E-mail address: harri.hakula@tkk.fi

AALTO UNIVERSITY, INSTITUTE OF MATHEMATICS, P.O. Box 11100, FI-00076 AALTO, FINLAND

E-mail address: antti.rasila@iki.fi

AALTO UNIVERSITY, INSTITUTE OF MATHEMATICS, P.O. Box 11100, FI-00076 AALTO, FINLAND

E-mail address: vuorinen@utu.fi

DEPARTMENT OF MATHEMATICS, FI-20014 UNIVERSITY OF TURKU, FINLAND